Electron-Positron Beams from Terrestrial Lightning Observed with Fermi GBM

Michael S. Briggs,[1] Valerie Connaughton,[1] Colleen Wilson-Hodge,[2]
Robert D. Preece,[1,3] Gerald J. Fishman,[2] R. Marc Kippen,[4]
P. N. Bhat,[1] William S. Paciesas,[1,3] Vandiver L. Chaplin,[1]
Charles A. Meegan,[5] Andreas von Kienlin,[6] Jochen Greiner,[6]
Joesph R. Dwyer[7] and David M. Smith[8]

Preprint, 2011 January 1

Terrestrial Gamma-ray Flashes (TGFs) are brief pulses of energetic radiation observed in low-earth orbit. They are associated with thunderstorms and lightning and have been observed both as gamma-ray and electron flashes depending on the position of the spacecraft with respect to the source. While gamma-ray TGFs are detected as short pulses lasting less than 1 ms, most TGFs seen by the Fermi Gamma-ray Burst Monitor (GBM) with durations greater than 1 ms are, instead, the result of electrons traveling from the sources along geomagnetic field lines. We perform spectral analysis of the three brightest electron TGFs detected by GBM and discover strong 511 keV positron annihilation lines, demonstrating that these electron TGFs also contain substantial positron components. This shows that pair production occurs in conjunction with some terrestrial lightning and that most likely all TGFs are injecting electron-positron beams into the near Earth environment.

1. Introduction

TGFs were unexpectedly discovered with the Burst and Transient Source Experiment (BATSE) on the Compton Gamma-Ray Observatory in the early 1990s [*Fishman et al.*, 1994]. Gamma-rays from TGFs have been observed to 40 MeV and higher [*Marisaldi et al.*, 2010a; *Briggs et al.*, 2010; *Marisaldi et al.*, 2010b]. Since their discovery with BATSE, TGFs have been associated with thunderstorms and lightning, an association that was strongly confirmed with the large sample from the Reuven Ramaty High Energy Solar Spectroscopic Imager (RHESSI) [*Smith et al.*, 2005]. The microphysics is believed to be well understood: electrons are accelerated to high energies in strong electric fields by the Relativistic Runaway Electron Avalanche (RREA) process, emitting gamma-rays via bremsstrahlung [*Gurevich et al.*, 1992; *Dwyer*, 2003]. When a spacecraft is located above the source, within a cone of $\approx 30°$ half-angle, a gamma-ray TGF may be observed.

Assuming a high-altitude source, *Lehtinen et al.* [2001] noted that some energetic electrons should also escape to space. Unlike photons, these charged particles are constrained to follow the geomagnetic field line, traveling helical paths. They predicted that the interactions of the electrons with the atmosphere at the geomagnetic conjugate point of the source would produce gamma-rays observable from a satellite; however, this gamma-ray glow has not yet been observed. Additionally, spectral fits of RHESSI data indicate a lower source altitude [*Dwyer and Smith*, 2005].

As the gamma-rays in a TGF propagate up and out of the atmosphere, they produce secondary electrons, mostly via Compton scattering and pair production. *Dwyer et al.* [2008] proposed that secondary electrons produced $\gtrsim 40$ km should escape into space, a mechanism that should take place regardless of the source altitude. Furthermore they proposed that the electrons could be observed by their directly interacting with an instrument located along the field line from the source. While gamma-rays disperse from the source, the intensity of an "electron TGF" is maintained with distance from the source because the electrons follow the field line; however electron TGFs are infrequently detected because the electron beam has a small diameter [*Dwyer et al.*, 2008; *Carlson et al.*, 2009]. This model additionally predicts that electron TGFs should have longer durations because of velocity dispersion due to the range of helical pitch angles: electrons with low pitch angles have velocities nearly aligned along the field line and arrive at the satellite first. Electrons with high-pitch angles have similar velocity magnitudes but have smaller velocity components along the field and arrive later. Furthermore, if the geomagnetic field at the conjugate point is stronger than at the source, electrons will magnetically mirror above the atmosphere and return along the field line to the satellite.

BATSE TGF 2221 and the RHESSI TGF of 17 January 2004 showed both signatures in their time histories, lengthening and a second peak [*Dwyer et al.*, 2008], as does Gamma-ray Burst Monitor (GBM) TGF 091214 (Fig. 1). All three of these TGFs were detected when the spacecrafts were over the Sahara desert, with the spacecrafts magnetically connected to the region of high thunderstorm activity in southern Africa. These events are identified as electron TGFs based on their time profiles and other characteristics; the detectors are unable to distinguish photons from electrons. The Solar Anomalous Magnetospheric Particle Explorer (SAMPEX) Heavy Ion Large Telescope (HILT) is sensitive to ions and electrons; with it numerous possible electron TGFs have been identified [*Carlson et al.*, 2009]. It is difficult to conclusively establish the nature of these events from the SAMPEX data alone because of the 20 ms resolution of that data. As additional confirmation that some TGFs have been observed via electrons directed along a geomagnetic field line, the associated lightning discharge at the terminus of the field line was observed for the first time for GBM TGF 100515 [*Cohen et al.*, 2010].

The Fermi Gamma-ray Space Telescope is in orbit at ≈ 560 km altitude and $25.6°$ inclination. Fermi consists of two instruments, the Large Area Telescope (LAT), a pair conversion telescope for observing above 20 MeV [*Atwood et al.*, 2009], and the Gamma-ray Burst Monitor. GBM consists of 14 detectors of two types arranged to view the unocculted sky: twelve sodium iodide (NaI) scintillator detectors cover the energy range ≈ 8 keV to 1 MeV, while two bismuth germanate (BGO) scintillator detectors cover the energy range ≈ 200 keV to ≈ 40 MeV [*Meegan et al.*, 2009]. These scintillation detectors record energy deposited by high-energy particles such as photons, protons and electrons; they do not distinguish among particle types. Even though TGFs originate from the Earth's atmosphere near the nadir, the radiation from TGFs is so penetrating that signals are typically produced in most of the GBM detectors. The GBM BGO detectors are well suited for TGF

[1]CSPAR, University of Alabama in Huntsville, Huntsville, AL, 35899, USA

[2]Space Science Office, NASA Marshall Space Flight Center, Huntsville, AL, 35812, USA

[3]Dept. of Physics, University of Alabama in Huntsville, Huntsville, AL, 35899, USA

[4]ISR-1, Los Alamos National Laboratory, Los Alamos, NM 87545, USA

[5]Universities Space Research Association, Huntsville, AL, 35803, USA

[6]Max-Planck Institut für extraterrestrische Physik, D-85741 Garching, Germany

[7]Physics and Space Sciences, Florida Institute of Technology, Melbourne, FL 32901, USA

[8]Dept. of Physics, University of California, Santa Cruz, Santa Cruz, CA 95064, USA

observations due their large volumes, high efficiency for detecting gamma-rays and good ability to measure the full energy of MeV gamma-rays. The improved sensitivity and absolute timing accuracy of GBM have already provided new results on TGFs. The time profiles are observed to be symmetric or to have faster rises than falls; one TGF had a rise time of only ≈ 7 μs. GBM has observed TGFs with partially overlapping pulses [*Briggs et al.*, 2010]. Thirteen GBM TGFs were found to be simultaneous to within ≈ 40 μs with radio-detected lightning discharges; clusters of lighting indicative of storms were found for additional TGFs [*Connaughton et al.*, 2010]. Properties of the first 50 GBM TGFs are summarized by *Fishman et al.* [2010].

2. Sample and Analysis

GBM detected 77 TGFs between 2008 July 11 and 2010 July 1. Figure 2 shows the duration distribution of these TGFs, using the t_{90} duration measure [*Koshut et al.*, 1996]. Most of the TGFs have t_{90} durations from 0.1 to 1.0 ms, with a small fraction contributing a tail to the distribution extending to 25 ms. Two of the eight TGFs with $t_{90} > 1$ ms consist of multiple separated short pulses – these two are gamma-ray TGFs. Based upon the velocity dispersion effect producing longer durations for electron TGFs the remaining six long TGFs are probably electron TGFs.

Here we investigate the spectra of the three brightest TGFs from this sub-sample of six TGFs (Table 1). These three TGFs, 080807, 090813 and 091214, were already identified as very likely electron TGFs [*Briggs et al.*, 2010; *Connaughton et al.*, 2010] based on several unusual characteristics that they share: they are unusually long, their spectra have maximum energies of ≈ 10 MeV compared to $\gtrsim 30$ MeV for most TGFs and using the World Wide Lightning Location Network (WWLLN), a network of VLF radio receivers [*Rodger et al.*, 2009], lightning discharges were observed within 50 km of one of the termini of the magnetic field lines through Fermi, but not underneath Fermi. The duration and two peaks of TGF 091214 are compellingly explained by charged particles arriving on the geomagnetic field line through Fermi (Fig. 1), strongly supporting the "electron" nature of this TGF. Mirror peaks were neither observed nor expected for TGFs 080807 and 090813. For these two TGFs, at equal altitudes, the magnetic field is weaker at the conjugate location so that particles penetrate farther into the atmosphere and are absorbed before they reach a field strong enough to cause mirroring.

Using lightning locations from WWLLN, the largest observed offset of a source of a GBM gamma-ray TGF from the sub-Fermi point is 300 km [*Briggs et al.*, 2010; *Connaughton et al.*, 2010][1]. The sources of these three TGFs (Table 1) range from 520 to 4300 km from Fermi so that Fermi should be outside of the gamma-ray beam and only charged particles are expected to be detected. We simulate the response of GBM to incident particles using GRESS [*Kippen et al.*, 2007], obtaining model count spectra. Separate simulations of 5×10^8 particles are made for each TGF and for electrons and positrons, and for various continuum spectra for the electrons and positrons. We find for the continuum spectra that an empirical model of an exponential shape, $A \exp(-E/E_0)$, matches the data well when the E-folding energy, E_0, is optimized. The simulation directs particles at Fermi from the direction of the magnetic field line from the source, using the field direction at the location of Fermi and assuming that all particle velocities are parallel to the field. Mixtures of these simulated count spectra are fit to the observed counts[2].

A surprising result is that the fits show the presence of both an electron component and a substantial positron component (Table 1). The positron component manifests itself as a strong 511 keV gamma-ray line (Fig. 3) produced when positrons annihilate with Fermi. Incident continuum photon spectra produce 511 keV lines from pair production in Fermi, but the lines are much weaker than those observed (Fig. 1 of the Auxiliary Material). Pure electron spectra should produce a 511 keV line from pair production from bremsstrahlung photons, however this feature is negligible in the model spectra (Fig. 2 of the Auxiliary Material). Positron fractions, $N(e^+)/(N(e^-) + N(e^+))$, range from ≈ 0.1 to ≈ 0.3. The values of the E-folding energy, E_0, of the continua range from 2.3 to 4.6 MeV (Table 1, Fig. 3 of the Auxiliary Material) – the electron/positron spectra of TGFs have lower exponential energies and lower maximum energies than the gamma-ray spectra [*Dwyer and Smith*, 2005; *Briggs et al.*, 2010; *Marisaldi et al.*, 2010a]. The 511 keV positron annihilation line and the lower maximum energy are visible in the raw data (Fig. 4 of the Auxiliary Material).

Table 1 lists the improvements in the fitting statistic, Δ(C-Stat), from adding positrons to electrons-only fits. We conducted simulations to demonstrate that these improvements are extremely unlikely by chance if only electrons are reaching Fermi and that therefore the detections of positrons are statistically significant. For each TGF, 25000 simulated spectra were created and then each of these simulated spectra were fit twice, with the electrons-only model and with the electrons+positrons model[3]. The C-Stat improvements from adding a positron component were always smaller in the simulations than for the real data, showing that the positron components have significances of at least 99.996% (Gaussian equivalent to 3.9σ). Furthermore, the three TGFs represent independent detections of positron components.

3. Conclusions

The detection of positrons arriving at Fermi from TGFs is direct evidence for a relativistic phenomenon occurring in conjunction with terrestrial lightning: pair production. These positrons are expected from interactions of the TGF gamma-ray propagating upwards, but the positron fraction is higher than anticipated by *Dwyer et al.* [2008]. Monte Carlo simulations now give values of $\approx 11\%$, depending on location in the beam, which is broadly consistent with the fitted values (Table 1). The discovery is strong confirmation that some TGFs are detected from electrons and positrons beamed along geomagnetic field lines from distant sources to the spacecraft, rather than from gamma-rays from sources beneath the spacecraft. The finding of high positron fractions, $\gtrsim 10\%$, in the three brightest electron TGFs detected by GBM suggests that all TGFs emit substantial numbers of positrons to space. Whether TGFs make an important contribution of electrons and positrons to the inner radiation belt depends on both the poorly known intensity distribution of TGFs and on the degree of scattering from the electron/positron beams. Without scattering, most of the particles will be absorbed into the atmosphere after one or, if mirroring occurs, two inter-hemispherical passages [*Lehtinen et al.*, 2000, 2001].

The future TGF missions Firefly and TARANIS include instruments with the capability to distinguish between photons and electrons, with TARANIS also including a high-energy electron instrument.

Notes

1. We use the GBM results for source/sub-satellite offsets in case there is an instrumental dependence.
2. Details of the fitting method are in the Auxiliary Material.
3. Further details on the simulations procedure are in the Auxiliary Material.

References

Atwood, W. B., A. A. Abdo, M. Ackermann, et al. (2009), The large area telescope on the Fermi gamma-ray space telescope mission, *ApJ*, *697*, 1071–1102, doi:10.1088/0004-637X/697/2/1071.

Briggs, M. S., et al. (2010), First results on terrestrial gamma-ray flashes from the fermi gamma-ray burst monitor, *J. Geophys. Res.*, *115*, A07,323, doi:10.1029/2009JA015242.

Carlson, B. E., N. G. Lehtinen, and U. S. Inan (2009), Observations of terrestrial gamma-ray flash electrons, in *Conf. Proc. 1118*, edited by N. B. Crosby, T.-Y. Huang, and M. J. Rycroft, pp. 84–91, AIP.

Cohen, M. B., R. K. Said, U. S. Inan, M. S. Briggs, G. Fishman, V. Connaughton, and S. A. Cummer (2010), A lightning discharge producing a beam of relativistic electrons into space, *Geophys. Res. Lett.*, *37*, L18,806, doi:10.1029/2010GL044481.

Connaughton, V., et al. (2010), Associations between fermi gbm terrestrial gamma-ray flashes and sferics from the wwlln, *J. Geophys. Res.*, *115*, A12,307, doi:10.1029/2010JA015681.

Dwyer, J. R. (2003), A fundamental limit on electric fields in air, *Geophys. Res. Lett.*, *30*, ASC8.1–ASC8.4, doi:10.1029/2003GL017781.

Dwyer, J. R., and D. M. Smith (2005), A comparison between monte carlo simulations of runaway breakdown and terrestrial gamma-ray flash observations, *Geophys. Res. Lett.*, *32*, L22,804, doi:10.1029/2005GL023848.

Dwyer, J. R., B. W. Grefenstette, and D. M. Smith (2008), High-energy electron beams launched into space by thunderstorms, *Geophys. Res. Lett.*, *35*, L02,815, doi:10.1029/2007GL032430.

Fishman, G. J., et al. (1994), Discovery of intense gamma-ray flashes of atmospheric origin, *Science*, *264*, 1313–1316.

Fishman, G. J., et al. (2010), Temporal properties of terrestrial gamma-ray flashes (tgfs) from the gamma-ray burst monitor on the fermi observatory, *J. Geophys. Res.*, *submitted*.

Gurevich, A. V., G. M. Milikh, and R. Roussel-Dupre (1992), Runaway electron mechanism of air breakdown and preconditioning during a thunderstorm, *Physics Letters A*, *165*, 463–468.

Kippen, R. M., et al. (2007), Instrument response modeling and simulation for the glast burst monitor, in *Conf. Proc. 921*, edited by P. M. . C. M. S. Ritz, pp. 590–591, AIP.

Koshut, T. M., W. S. Paciesas, C. Kouveliotou, and J. van Paradijs (1996), Systematic effects on duration measurements of gamma-ray bursts, *ApJ*, *463*, 570–592.

Lehtinen, N. G., U. S. Inan, and T. F. Bell (2000), Trapped energetic electron curtains produced by thunderstorm driven relativistic runaway electrons, *Geophys. Res. Lett.*, *27*, 1095–1098.

Lehtinen, N. G., U. S. Inan, and T. F. Bell (2001), Effects of thunderstorm-driven runaway electron electrons in the conjugate hemisphere, *J. Geophys. Res.*, *106*, 28,841–28,856, doi:10.1029/2000JA000160.

Marisaldi, M., F. Fuschino, C. Labanti, M. Galli, F. Long, E. D. Monte, et al. (2010a), Detection of terrestrial gamma-ray flashes up to 40 MeV by the AGILE satellite, *J. Geophys. Res.*, *115*, A00E13, doi:10.1029/2009JA014502.

Marisaldi, M., A. Argan, A. Trois, A. Giuliani, M. Tavani, C. Labanti, F. Fuschino, et al. (2010b), Gamma-ray localization of terrestrial gamma-ray flashes, *Phys. Rev. Lett*, *105*, 128,501, doi:10.1103/PhysRevLett.105.128501.

Meegan, C. A., et al. (2009), The Fermi gamma-ray burst monitor, *ApJ*, *702*, 791–804, doi:10.1088/0004-637X/702/1/791.

Rodger, C. J., J. B. Brundell, R. H. Holzworth, and E. H. Lay (2009), Growing detection efficiency of the world wide lightning location network, in *Conf. Proc. 1118, Coupling of Thunderstorms and Lightning Discharges to Near-Earth Space*, edited by N. B. Crosby, T.-Y. Huang, and M. J. Rycroft, pp. 15–20, AIP.

Smith, D. M., L. I. Lopez, R. P. Lin, and C. P. Barrington-Leigh (2005), Terrestrial gamma-ray flashes observed up to 20 MeV, *Science*, *307*, 1085–1088.

————————

P. N. Bhat, M. S. Briggs, V. L. Chaplin, V. Connaughton, W. S. Paciesas and R. D. Preece, CSPAR, 320 Sparkman Drive, Huntsville, AL, 35805, USA. (michael.briggs@uah.edu).

G. J. Fishman and C. Wilson-Hodge, Space Science Office, VP62, NASA Marshall Space Flight Center, Huntsville, AL, 35812, USA. (jerry.fishman@nasa.gov)

R. M. Kippen, ISR-1, Los Alamos National Laboratory, Los Alamos, NM 87545, USA. (mkippen@lanl.gov)

C. A. Meegan USRA, 320 Sparkman Drive, Huntsville, AL, 35805, USA. (chip.meegan@nasa.gov).

J. Greiner and A. von Kienlin, Max-Planck Institut für extraterrestrische Physik, D-85741 Garching, Germany. (azk@mpe.mpg.de)

J. R. Dwyer, Physics and Space Sciences, Florida Institute of Technology, Melbourne, FL 32901, USA. (jdwyer@fit.edu)

D. M. Smith, Dept. of Physics, University of California, Santa Cruz, Santa Cruz, CA 95064, USA. (dsmith@scipp.ucsc.edu)

Table 1. Properties of the three brightest GBM electron TGFs.

Trigger	Date	Trigger Time (UT)	t_{90} (ms)	t_{90} counts[b]	Fermi position E. Long. (°)	Lat. (°)	Likely Source[a] E. Long. (°)	Lat. (°)	Conjugate[a] E. Long. (°)	Lat. (°)
080807.357	2008 Aug 07	08:33:24.191042	3.08	353	253.01	+15.30	253.69	+20.00	242.85	-34.45
090813.215	2009 Aug 13	05:10:14.790074	3.84	528	278.29	-2.19	278.17	+7.00	276.03	-30.68
091214.495	2009 Dec 14	11:53:27.829662	25.92	1735	31.42	+25.34	31.93	-13.13	31.73	+30.45

Trigger	Interval fit[c] (ms)	BGO 0 counts[f]	gain[d] corr.	E_0 (MeV)	positron fraction	Δ(C-Stat)[e]
080807.357	−10.5 to −6.5	98	0.95	2.3	0.099 ± 0.022	54.2
090813.215	−15.5 to −12.0	75	0.95	4.6	0.34 ± 0.08	42.8
091214.495	−1.0 to +5.0	107	0.925	3.0	0.19 ± 0.04	47.0

[a] Calculated using the 11th Generation International Geomagnetic Reference Field (IGRF-11) (`http://www.ngdc.noaa.gov/IAGA/vmod/igrf.html`) and a 30 km altitude. The source region for the electrons and positrons extends above this altitude along the field line.

[b] Sum over all 14 GBM detectors of all counts within the t_{90} interval, except for TGF 080807, for which only the detectors on the $+X$ side of the spacecraft are included.

[c] Relative to the trigger time.

[d] A gain correction factor less than one increases the gain of the model by scaling the energy edges of the channels when the model counts are binned, implying that the observed annihilation line is at a higher than expected energy.

[e] Improvement of C-Stat for the electron+positron fit relative to the electron-only fit.

[f] The counts used for the spectral fits: sum of all counts in BGO 0 in the time interval and energy channel range used for the fits.

Figure 1. Left: The geometry of TGF 091214, projected onto the plane that includes both the axis of the Earth and Fermi. The coordinate z measures height along the Earth's axis and the coordinate r measures distance from the Earth's axis. The curve shows the geomagnetic field line through Fermi (blue dot) using the IGRF-11 model. Right: Black histogram: the time history of TGF 091214 as observed by GBM, summed over all 14 detectors. Magenta histogram: A Monte Carlo simulation of TGF 091214 that includes the relevant physical processes [*Dwyer*, 2003]. The adjustable parameters are the location of the source with respect to the field line through Fermi, the onset time of the TGF, the intensity of the TGF and the GBM background level. The electrons and positrons travel 5490 km from the TGF source over Zambia (solid red dot) to Fermi over southern Egypt (blue dot), with velocity dispersion acting over this distance to stretch the source pulse to ≈20 ms. Additional particles mirror over northern Egypt (red circle), returning to Fermi to produce the second pulse.
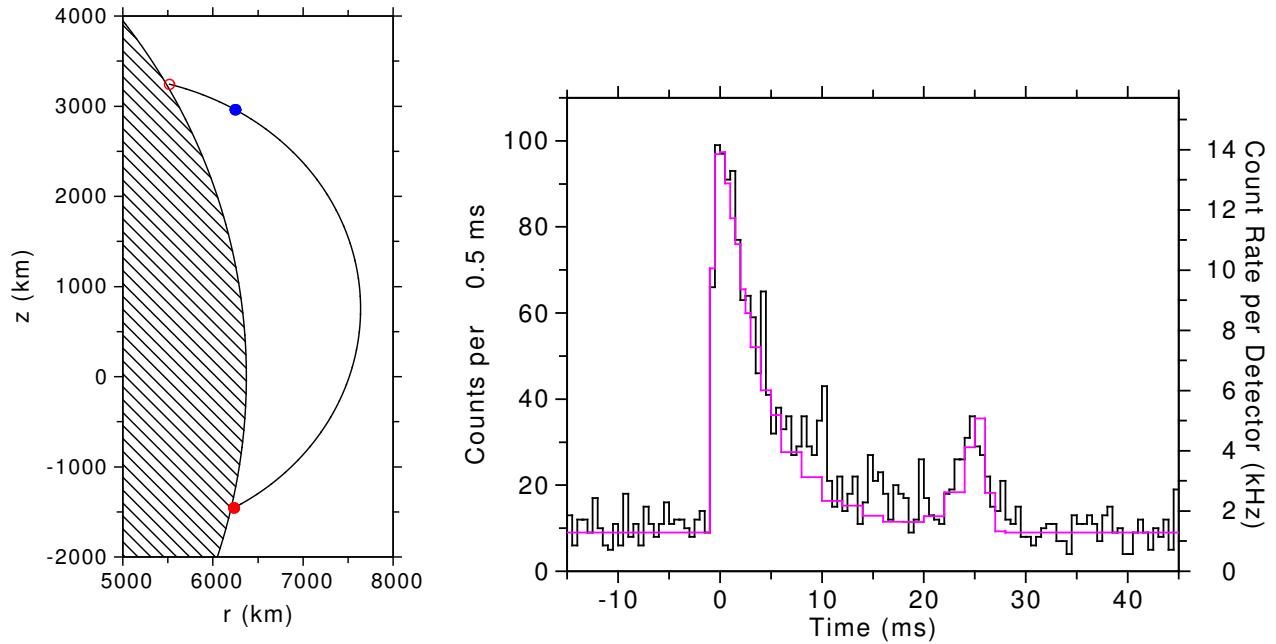
Figure 2. t_{90} duration distribution for 77 GBM TGFs. The t_{90} measure is the length of the central interval containing 90% of the counts, starting from the time of 5% of the counts and ending at the time of 95% of the counts [*Koshut et al.*, 1996]. For TGFs we omit inter-pulse gaps from the t_{90} value.
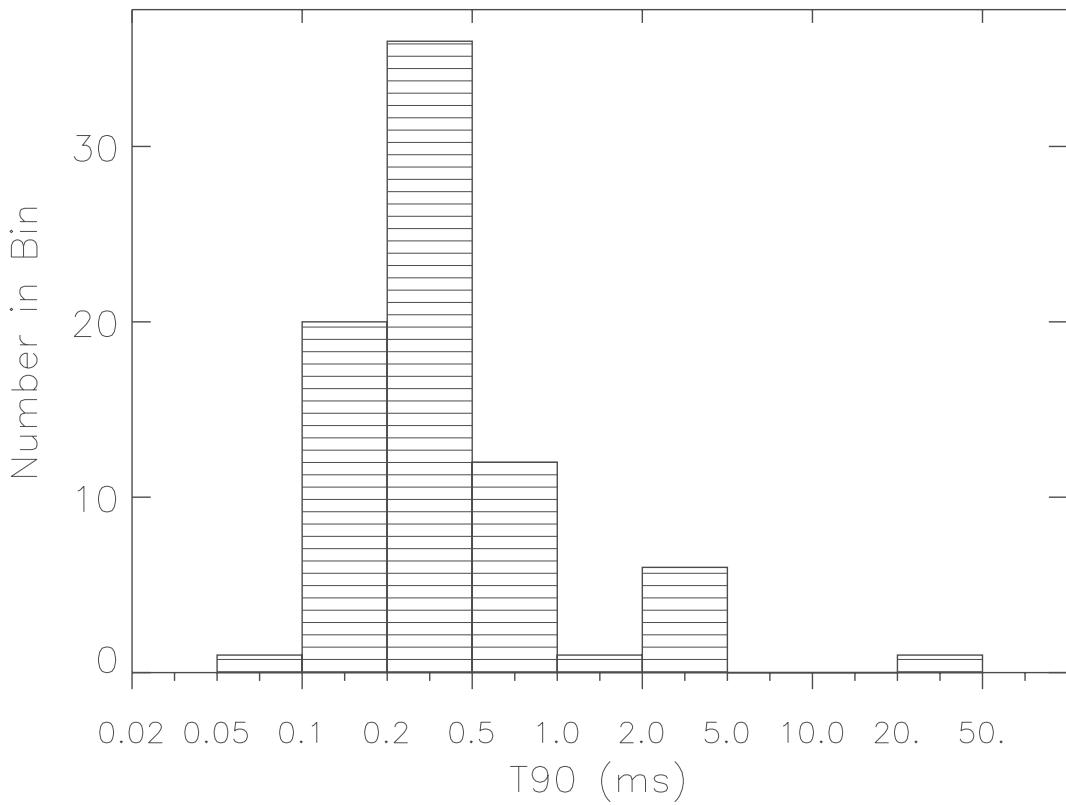
Figure 3. Spectral data (magenta points) and model fits (blue histograms) for TGFs 080807, 090813 and the first pulse of 091214. The plots for TGFs 080807 and 091214 are shifted by factors of fifty to avoid overlapping. Data points within 1σ of zero are displayed as 2σ upper-limits (T-symbols). The models are the best-fit mixtures of electrons and positrons (Table 1), converted into expected counts in BGO detector 0 with GRESS simulations (see Auxiliary Material).
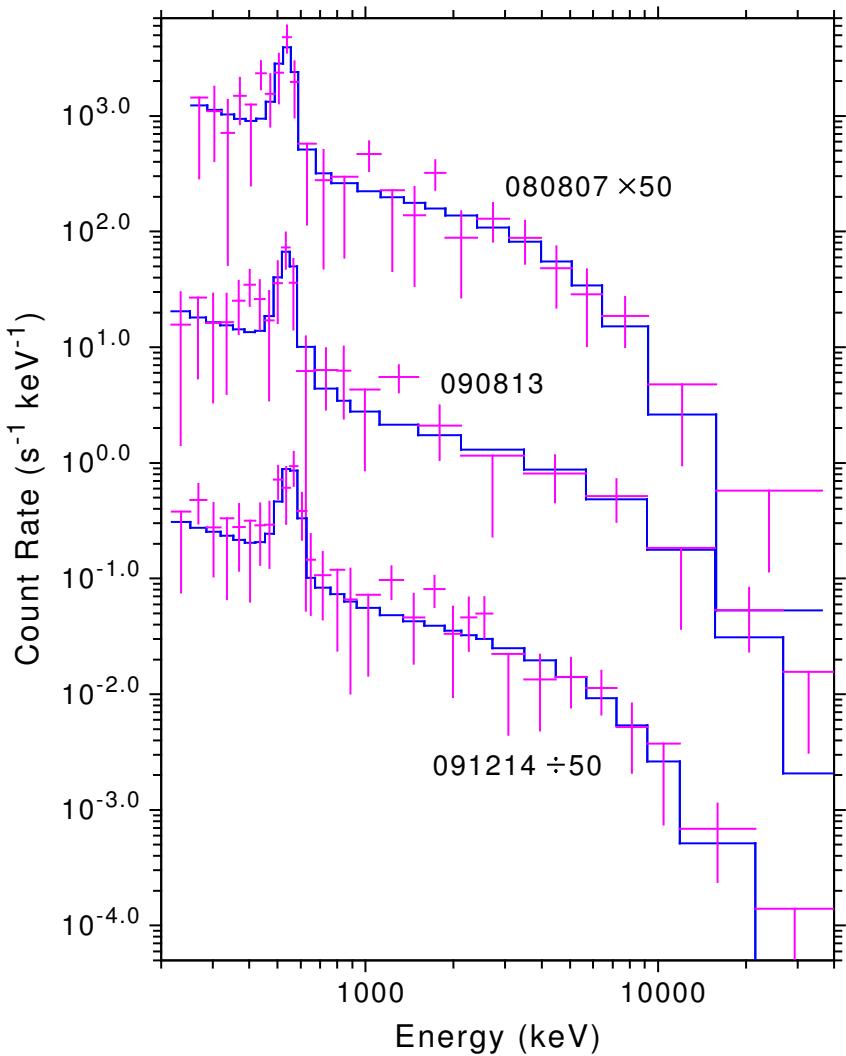
Auxiliary Material

for

Electron-Positron Beams from Terrestrial Lightning
Observed with Fermi GBM

by M. S. Briggs, V. Connaughton, C. Wilson-Hodge,
R. D. Preece, G. J. Fishman, R. Marc Kippen,
P. N. Bhat, W. S. Paciesas, V. L. Chaplin,
C. A. Meegan, A. von Kienlin, J. Greiner,
J. R. Dwyer and D. M. Smith

1. Spectral Fitting Details

We use the data from the GBM BGO detectors for the spectral fits since, compared to the GBM NaI detectors, the BGO detectors have higher effective areas and higher probabilities of absorbing 100% of the photon's energy [*Meegan et al.*, 2009]; by coincidence, the first pulse of TGF 091214 and the other two TGFs were all best observed with BGO 0. Background is obtained from ±10 s of data, omitting a short interval containing the TGF.

The lines in the BGO 0 data appear to be above 511 keV by 5% to 7.5%. This cannot be a property of the TGFs since the positrons are annihilating on Fermi and no shift of the centroid is expected. The gain of the BGO detectors is controlled by the location of a 2.2 MeV line in the background; this control may be off by ≈1%. It may be that the calibration of the BGO detectors needs to be improved. The models have been gain-adjusted to agree with the annihilation lines in the data (Main Paper Fig. 3, Table 1).

Spectral analysis of GBM data is normally done using response matrices that encode the response of GBM to photons. That method is inappropriate for these TGFs since GBM detected charged particles rather than photons. Instead the response of the GBM detectors to particles incident on Fermi is found by performing simulations using GRESS [*Kippen et al.*, 2007] (`http://public.lanl.gov/mkippen/gress/versions.html`), an adaption of Geant4 [*Agostinelli et al.*, 2003]. The fits are made using a customized version of rmfit 3.2 in which the models are count rate templates produced from the GRESS simulations. This is a forward-folding method since the count data are fit to count models based on the instrumental response to the assumed electron and positron spectral models. We use the Castor C-Stat statistic (`http://heasarc.gsfc.nasa.gov/docs/xanadu/xspec/XspecManual.pdf`), which is the same as Poisson log-likelihood, except for an offset which is constant for each dataset. Based upon a model with selected components (e.g., electrons and positrons) and properties (E_0 and gain correction factor), the non-linear fitting program rmfit optimizes the amplitudes of the components so as to minimize C-Stat.

The fitting program cannot directly optimize two additional parameters, the TGF continuum spectrum parameter E_0 (see main text) and the detector gain correction factor, because the values of these parameters must be assumed in order to create model count spectra with GRESS. Instead, we create a series of model count spectra for various values of E_0 and the gain correction factor. Each pair of electron and positron model count spectra, with particular values of E_0 and gain, are fit to optimize the mixture of electrons and positrons. We always use the same values of E_0 and gain for the electron and the positron components. From these fits, the one with the lowest C-Stat value determines the best values of E_0 and the gain correction factor (Table 1 and Auxiliary Fig. 3), but only over the discrete values for which model spectra were created.

While it is natural that the detector gain correction factor should be the same for both components since this is a detector property, it is not necessary that both components have the same value of E_0 as assumed. The positrons are produced by pair production, while the electrons are produced by Compton scattering and pair production. The simplifying assumption of common values of E_0 resulted in excellent fits for these three TGFs. In future work we will to abandon the empirical exponential-continuum model and the approximation that all particles arrive along the magnetic field line, switching to spectra and particle directions obtained from Monte Carlo simulations of TGFs. While the derived value of the positron fraction is largely determined by the strength of the 511 keV line, as long as the assumed continuum model is a good fit, changing the assumed continuum model may cause a small change in the positron fraction.

While the fits are made using the data at its intrinsic energy channel resolution, higher channels are rebinned into wider intervals for the plots (Main Paper Fig. 3 & Auxiliary Figs. 1 & 2). The rebinning begins above the line and progressively more channels are summed at higher energies. Without this rebinning, the higher channels would appear on the plots as numerous non-informative upper-limits.

2. Simulation Details

For each TGF, 25000 simulated spectra were made using random Poisson deviates based on the spectral parameters of the best electrons-only fits to the real data. Each of these simulated spectra were fit twice, with the electrons-only model and with the electrons+positrons model. Because C-Stat is equivalent to -2 log-likelihood, the difference in C-Stat between two models, Δ(C-Stat), is a likelihood ratio. Comparing these two models can therefore be done as a Likelihood Ratio Test. Here the null hypothesis is that the signal is due to electrons only, and the more complicated model is that the signal is due to electrons and positrons. The goal is to demonstrate that the more complicated model is statistically significant.

Adding a positron component to the simulated spectra, created assuming the null hypothesis of only electrons, never resulted in an improvement in Δ(C-Stat) as large as obtained in fitting the actual data, showing that the improvements Δ(C-Stat) (Table 1) for the actual data are improbable as chance fluctuations at $P \leq 1/25000$ and that the positron components are significant at the 99.996% confidence level or better.

We used simulations to show that the improvements in C-Stat (Table 1) are not due to chance and that therefore the positron component in the fits is statistically significant for two reasons. The usual method for Likelihood Ratio tests obtains a probability that the likelihood improvement between the null hypothesis (assumed true) and the more general hypothesis by a calculation based on the likelihood ratio being distributed as χ^2_m, where m is the number of additional parameters of the more complicated model (here $m = 1$) [*Martin*, 1971; *Eadie et al.*, 1971]. If this probability is very low the assumption that the null hypothesis is true will be contradicted and the positron component will be significant at the level one minus that probability. However, two assumptions required for Δ(C-Stat) to be distributed as χ^2_1 are likely violated for the GBM TGF spectral fits: first, the theorem is asymptotic, but only $\sim$100 counts are used in these fits. Secondly, for the theorem to be applicable, the more complicated hypothesis cannot convert into the simpler one by setting a parameter to a value on the boundary of its allowed parameter space [*Protassov et al.*, 2002]. The second assumption is violated for the comparison of the electron and electron+positron models because the more complicated mixture model, with parameter space $f_{e+} \geq 0$ and $f_{e-} \geq 0$, converts into the simpler one by setting the weight of the positron component, f_{e+}, to zero. Lacking a mathematical prediction for the distribution of Δ(C-Stat) under the null hypothesis that only electrons are actually present we must instead use simulations to demonstrate the statistical significance of the positron component.

References

Agostinelli, S., et al. (2003), GImage 4a simulation toolkit, *Nuclear Instruments and Methods A*, *506*, 250–303, doi:10.1016/ S0168-9002(03)01368-8.

Briggs, M. S., et al. (2010), First results on terrestrial gamma-ray flashes from the fermi gamma-ray burst monitor, *J. Geophys. Res.*, *115*, A07,323, doi:10.1029/2009JA015242.

Eadie, W. T., E. Drijard, F. E. James, M. Roos, and B. Sadoulet (1971), *Statistical Methods in Experimental Physics*, Elsevier Sciencie, Amsterdam.

Kippen, R. M., et al. (2007), Instrument response modeling and simulation for the glast burst monitor, in *Conf. Proc. 921*, edited by P. M. . C. M. S. Ritz, pp. 590–591, AIP.

Martin, B. R. (1971), *Statistics for Physicists*, Academic Press, London.

Meegan, C. A., et al. (2009), The Fermi gamma-ray burst monitor, *ApJ*, *702*, 791–804, doi:10.1088/0004-637X/702/1/791.

Protassov, R., D. A. van Dyk, A. Connors, V. L. Kashyap, and A. Siemiginowska (2002), Statistics, handle with care: Detecting multiple model components with the likelihood ratio test, *ApJ*, *571*, 545–559.

_____

Figure 1. The TGF spectra fit using models with only photons incident on Fermi. The data are the same as in Main Paper Fig. 3, but the fit is based upon photons arriving from beneath Fermi. A more general continuum shape is used which can represent bremsstrahlung emission, $E^{-\lambda} \exp(-E/E_0)$. The best-fit count model (blue histogram) based upon incident photons includes a very weak 511 keV line from pair production in the detectors and the spacecraft. This line is far weaker than the 511 keV line present in the data (magenta points).
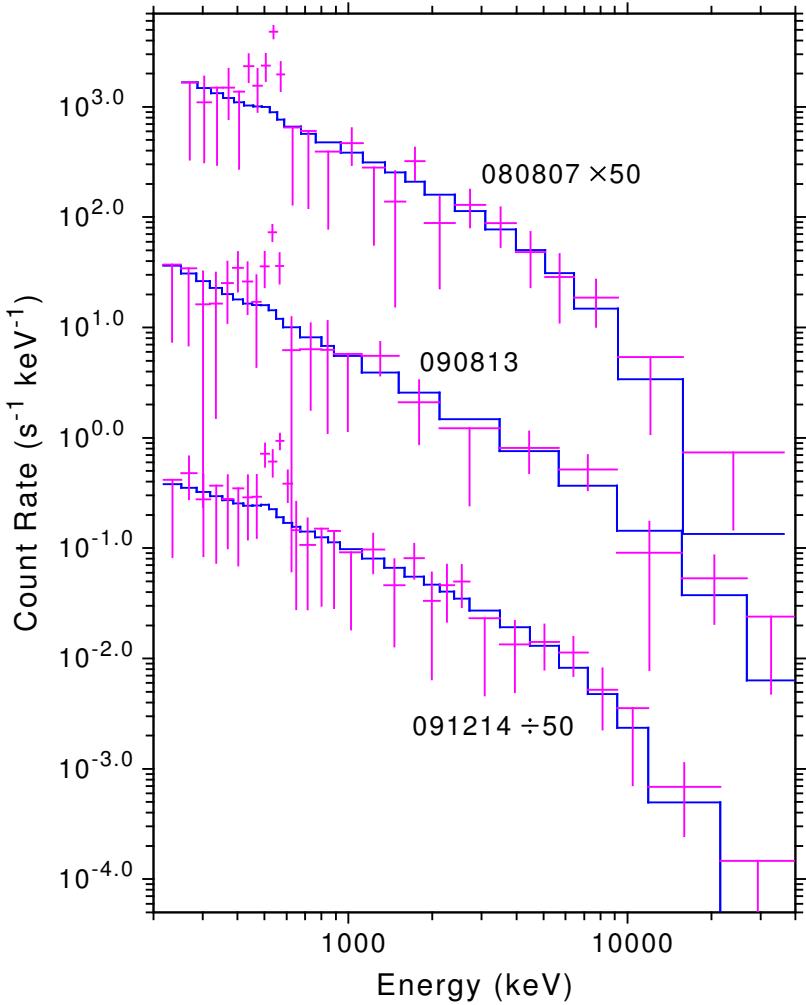
Figure 2. The TGF spectra fit using models with only electrons incident on Fermi. The data are the same as in Main Paper Fig. 3, but unlike the models of that figure, no positron component is included in the model spectra shown here. The best-fit electrons-only model (blue histogram) is clearly inconsistent with the data (magenta points).
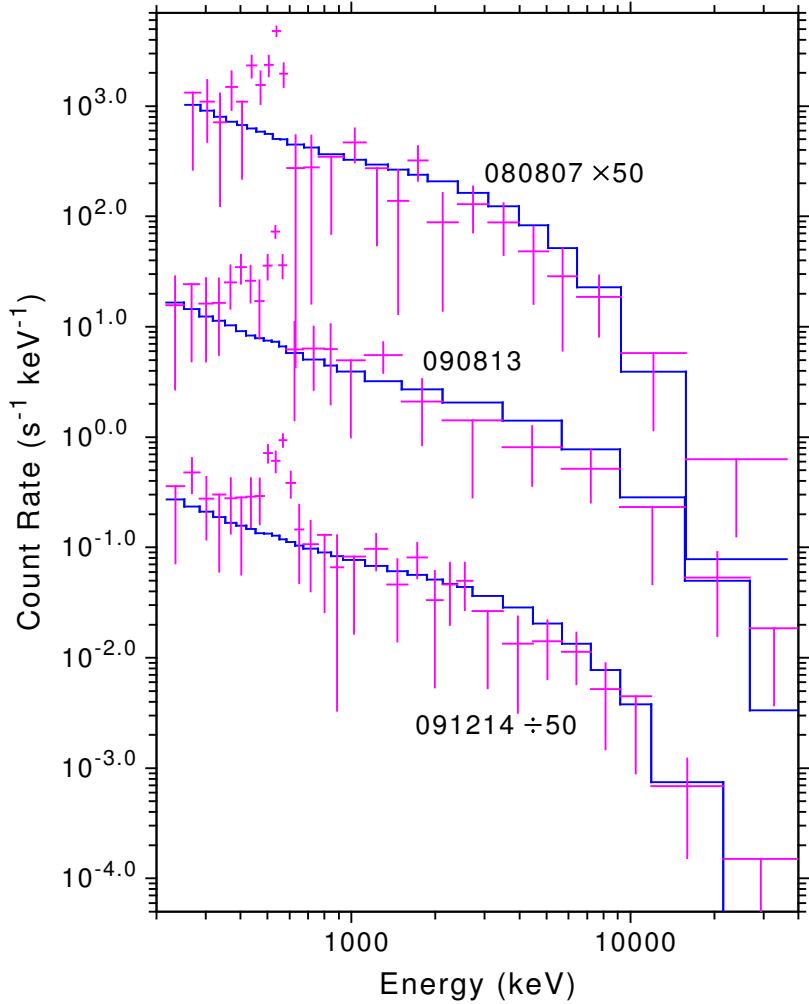
Figure 3. Graphs of C-Stat versus continuum E-folding energy E_0 created from a series of fits using model spectra produced for each value of E_0 that appears on a graph. The minima of C-Stat on these graphs determine the best-fit values of E_0 (Table 1).
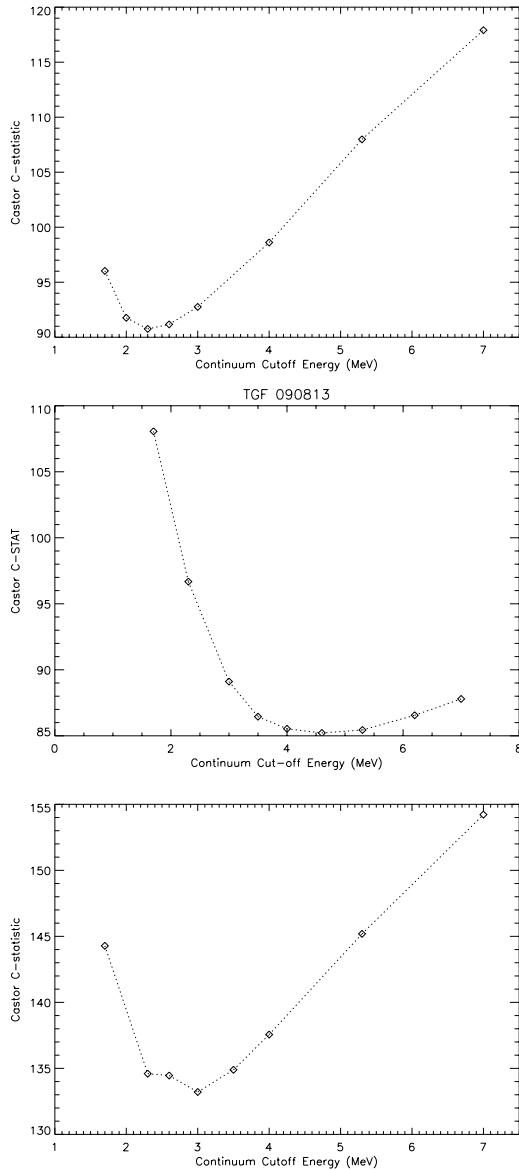
Figure 4. Scatter plots of individual counts observed with GBM detector BGO 0 for TGFs 080807, 090813 and 091214. Counts are the energy deposits of individual events – mostly individual photons but also including background events. For photons, the measured energy of the count is usually the same as that of the photon to within the detector resolution, but sometimes the detected energy of the count can be substantially less then the photon energy. The positron annihilation line is apparent as the horizontal "ridge" of points at 511 keV. These graphs also show that the maximum detected energies for TGFs 080807 and 091214 are about 10 MeV, substantially lower than that of gamma-ray TGFs (noted earlier for TGF 080807 *Briggs et al.* [2010]). The several counts at approximately channel 127 are overflow counts that are most likely due to cosmic rays rather than originating from the TGFs.